ARCHIVES OF ELECTRICAL ENGINEERING VOL. XX(Y), pp. 1-22 (2025)

This paper has been accepted for publication in the AEE journal. This is the version which has not been fully edited and content may change prior to final publication.
Citation information: DOI 10.24425/aee.2025.153901

Influence of winding configuration on properties of the multichannel permanent magnet brushless generator

KRYSTYNA KRZYWDZIŃSKA-KORNAK*, MARIUSZ KORKOSZ, JAN PROKOP

Faculty of Electrical and Computer Engineering
Rzeszow University of Technology
Al. Powstańców Warszawy 12, 35-959 Rzeszów, Poland
*e-mail: {*krzywdzinska/mkosz/jprokop}@prz.edu.pl*

Abstract: In order to enhance operational reliability, modifications to the design of machine windings are necessary. One of the methods of improving machine operational reliability is adapting the windings to accommodate multichannel operation. This paper presents the design and construction of a prototype multi-channel brushless generator with surface-mounted permanent magnets (MCBLPMG SPMs). It also discusses the findings of a research project aimed at examining the impact of different winding configurations on the properties of multichannel operation in the MCBLPMG SPM. The quad-channel solution allows for the implementation of three varying winding configurations. A mathematical model of the three-phase MCBLPMG was developed for the purpose of analysis. The configurations differ in terms of the placement of the individual phases within the channels. A series of numerical tests were conducted on the selected configurations. Furthermore, the results of laboratory tests are presented. The configurations analysed in single-channel operation (SCO) showed no effect on generator efficiency. However, certain configurations may induce asymmetric operation, depending on their design.

Key words: brushless machine, magnetic coupling, multichannel, permanent magnets generator, redundancy system, single-channel operation, winding configuration

1. Introduction

It is beyond doubt that brushless machines with permanent magnets are highly useful in a wide range of applications. The most significant advantage of these machines is their high energy conversion efficiency. The key factor contributing to this high efficiency is the use of permanent magnets made of rare earth elements. This high energy conversion results in a high volumetric power density of the unit. Like any electrical machine, a brushless permanent magnet machine (BLPMM) can also operate as a generator, serving as a source of electricity [1–11]. According to the specific requirements of the intended application, the BLPMM is also capable of operating in motor/generator mode [2–6]. Article [3] analysed the application of the machine in an unmanned aerial vehicle in terms of motor/generator operation. In the context of aircraft

This paper has been accepted for publication in the AEE journal. This is the version which has not been fully edited and content may change prior to final publication.
Citation information: DOI 10.24425/aee.2025.153901

applications, a BLPMM can often be used as a starter/generator [4–6]. Generally, in aircraft applications, a BLPMM operates as a generator continuously, except for a short period of time when it is used as a starter. Generators are used to power various floating objects, including those on the sea surface and those submerged underwater [7]. Another application is the use of BLPMMs in flywheel energy storage systems [8]. Furthermore, the literature highlights a notable increase in interest in using BLPMMs in wind turbine applications [9–12, 38]. Depending on the circumstances, the operation may be carried out within a grid network, as highlighted in article [12] or as a standalone operation as presented in references [4–7]. In the case of a standalone operation, the generator is responsible for supplying a specific receiver. In some instances, the receivers of electricity are critical, such as onboard equipment, medical equipment in hospitals, military devices, etc. In these instances, the term "critical drive" may be used. The certainty and reliability of the generator's operation are of considerable importance in such cases. Essentially, redundancy can be achieved by using two independent generators, which is the most flexible and reliable approach. However, it requires considerably more space for installation, such as, for instance, in an aircraft. In situations where space is limited, a more streamlined approach can be adopted. In such cases, a generator with improved fault tolerance can be employed. Improvements in generator reliability can be achieved in two ways. First, a multiphase solution can be used [13–25]. A review of the literature on multiphase machines reveals a dominance of publications on motor operation [13–24]. Employment of multiphase solutions in motors generally results in a reduction in the ripple of electromagnetic torque [16, 22, 24]. An increase in the number of motor phases enables the implementation of more sophisticated control methodologies [21]. This has the effect of considerably reducing the impact of the absence of, for instance, one or two phases on the electromagnetic torque generated [17–19, 23]. In article [25], the subject of using a multiphase solution for generator operation underwent an analysis. The addition of an increased number of phases for standalone operation serves to reduce the output voltage ripple of the DC circuit.

An intermediate solution between multiphase and multichannel designs is a dual-stator construction, as proposed in [26]. The loss of the entire winding allows the generator output voltage to be maintained while limiting output power. However, such designs are characterised by a high level of construction complexity.

The second case is based on the use of electrically independent channels within a single stator [27–33]. The application of multichannel (MC) solutions represents a relatively novel approach to achieving an acceptable level of redundancy in system operation. Similarly to multiphase solutions, motor operation is more frequently analysed [27–30]. However, a notable gap in the literature is the analysis of multichannel solutions in the context of generator operation. Only a limited number of articles address this issue, as highlighted in references [31–33]. In paper [31] on dual-channel switched reluctance generators, it was demonstrated that the configuration of the windings can significantly impact the performance of single-channel operation. A magnetically integrated charger using an MC solution is presented in [32]. Article [33] presents an analysis of the dual-channel operating conditions. MC solutions offer enhanced operational flexibility and a wider range of configuration possibilities.

This paper has been accepted for publication in the AEE journal. This is the version which has not been fully edited and content may change prior to final publication.
Citation information: DOI 10.24425/aee.2025.153901

Papers [34–39] analyse various types of windings used in electrical machines. In general, three solutions are used for windings construction. The first solution involves the use of distributed windings [34–36]. In cases where there is a reduced number of stator slots or a considerable number of rotor poles, concentrated windings are the optimal choice, as demonstrated by the findings presented in [34–36, 38, 39]. An alternative solution is toroidal winding [37].

A review of the existing literature reveals a lack of comprehensive publications that demonstrate the fundamental aspects of winding configuration options in multichannel machines. In the typical implementation of distributed windings, a full-pitch, fractional-pitch coil, or a very short-pitch winding is used. The authors consider this methodology to be inappropriate to achieve improvements in machine reliability.

The objective of this study is to analyse the winding configurations of a multichannel brushless permanent magnets generator (MCBLPMGs) in order to determine its properties. The generator has been designed to improve its operational reliability. In this case, a very short-pitch winding was applied, representing a novel approach to the subject. In the authors' opinion, this method enables three varying winding configurations for the MCBLPMG. This is of significant importance in the context of dual-channel operation. Those three configurations differ in the arrangement of the phase windings for each channel on the stator circuit of the machine. A comparative analysis was conducted, where each variant was evaluated in a selected state of generator operation (SCO). A mathematical model of the MCBLPMG has been developed, and numerical calculations along with selected laboratory tests have been performed.

2. Construction of the MCBLPMG SPM and configuration of channel windings

2.1. Construction of the MCBLPMG

A brushless machine with permanent magnets has been designed to operate as a multichannel machine. Figure 1(a) illustrates the geometry of the tested machine, with the various phases of the MCBLPMG highlighted in different colours. Figure 1(b) shows the prototype of the MCBLPMG.

This paper has been accepted for publication in the AEE journal. This is the version which has not been fully edited and content may change prior to final publication.
Citation information: DOI 10.24425/aee.2025.153901

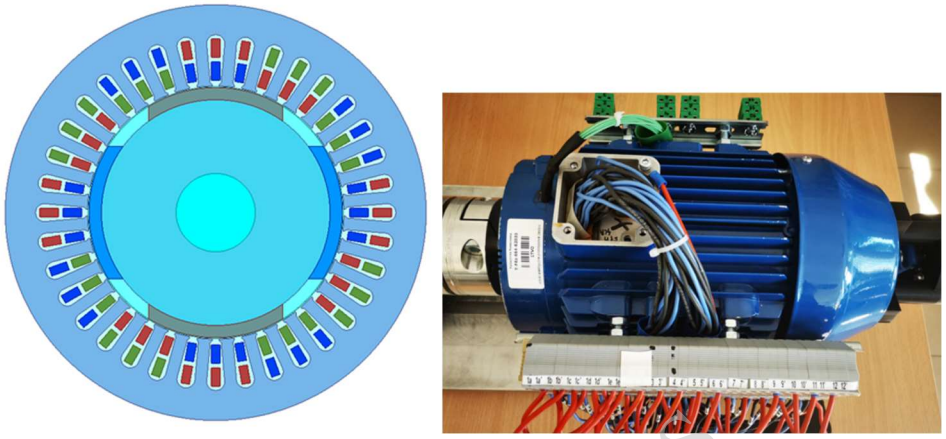

(a) (b)

Fig. 1. MCBLPMG: (a) geometry; (b) prototype

The machine has been designed to be capable of multichannel operation, specifically quad-channel operation. The essential short-pitch winding has been used, which is not a typical methodology in the design process. As a result, it is possible to configure the phase windings to create individual channels. The selected parameters of the test machine are presented in Table 1.

Table 1. Selected parameters of the MCBLPMG

No.	Parameter	Value	Unit
1	Number of phases	3	-
2	Number of channels	4	-
3	Number of stator slots	36	-
4	Number of rotor poles	4	-
5	Stator diameter	140	mm
6	Rotor diameter	81.5	mm
7	Air gap	0.5	mm
8	Active length	140	mm
9	Permanent magnet	N48SH	-
10	Magnet segments	4	-
11	Magnet skew	7.5	°*
12	Number of turns per channel	132	-
13	Number of coils per channel	3	-

This paper has been accepted for publication in the AEE journal. This is the version which has not been fully edited and content may change prior to final publication.
Citation information: DOI 10.24425/aee.2025.153901

14	Winding throw	3	-
15	Winding layers	2	-

where * – designed

2.2. Analysed channel winding configurations

The MCBLPMG design allows for quad-channel operation, with individual channels marked as A, B, C and D. The following operating models are possible in the quad-channel variant:

– Quad-Channel Operation (QCO),
– Triple-Channel Operation (TCO),
– Double Dual-Channel Operation (DDCO),
– Dual-Channel Operation (DCO),
– Double Single-Channel Operation (DSCO),
– Single-Channel Operation (SCO).

When a single energy receiver is in operation, all available operational modes can be applied. Additionally, the MCBLPMG is capable of operating with two independent energy receivers.

If the energy receiver is a battery bank, using an AC/DC system is recommended. This would allow for the implementation of an independent AC/DC system for each channel (four systems in total) or, alternatively, a simplified approach using only two AC/DC systems. In the second approach, two channels would be connected to each AC/DC system. The block diagram of the considered AC/DC system for SCO is illustrated in Fig. 2.

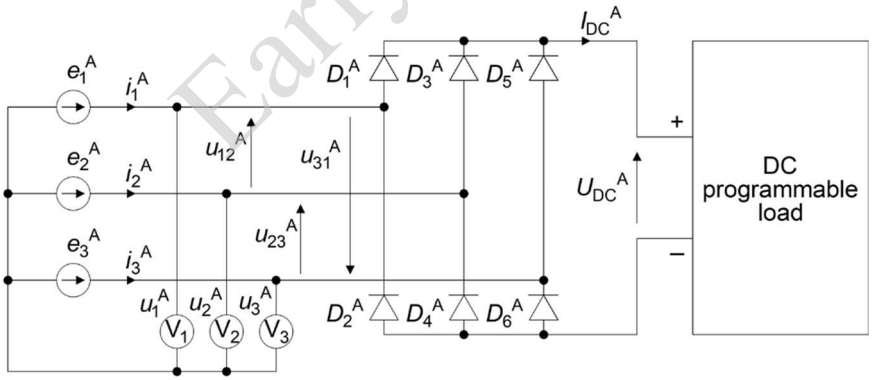

Fig. 2. Block diagram for SCO mode

The configuration of the channel for the individual phases in relation to the machine's stator parameters is of paramount importance, regardless of the operating mode. Three selected channel arrangement variants are possible:

– Var I with a geometrical shift equalling 120° (Fig. 3(a)),
– Var II with a geometrical shift equalling 60° (Fig. 3(b)),
– Var III with a geometrical shift equalling 30° (Fig. 3(c)).

This paper has been accepted for publication in the AEE journal. This is the version which has not been fully edited and content may change prior to final publication.
Citation information: DOI 10.24425/aee.2025.153901

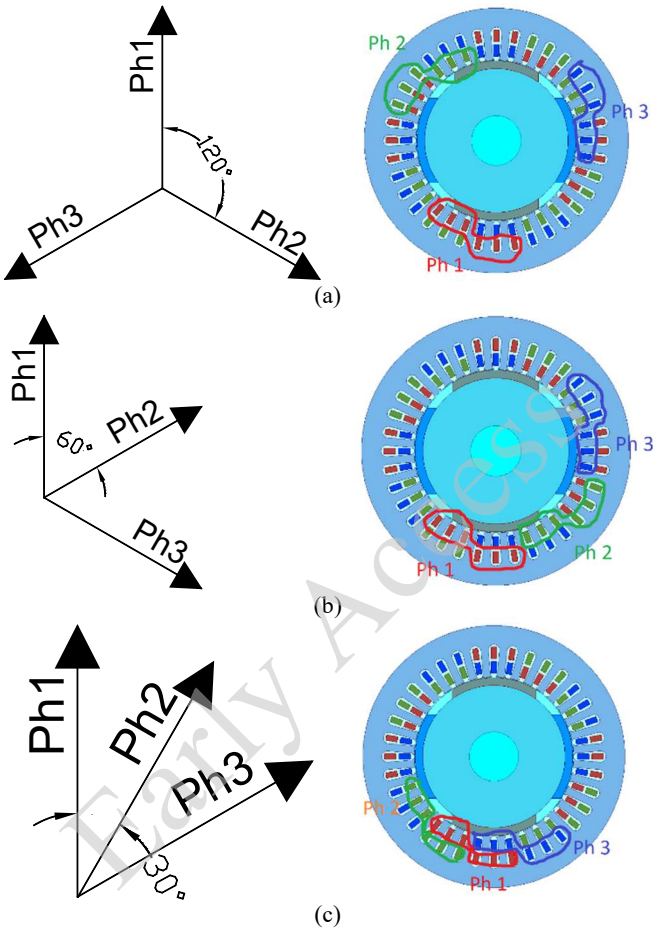

Fig. 3. The channel arrangement consists of: (a) Var I; (b) Var II; (c) Var III

In Var I (Fig. 3(a)), the phase windings of each channel arrangement are symmetrically distributed around the entire circumference. In Var III (Fig. 3(c)), all phases of a given channel are concentrated within the smallest possible angular span (half-pitch of the slot), achieving maximal concentration.

3. Mathematical model of the MCBLPM generator

The mathematical model of a three-phase MCBLPMG is presented for the QCO mode. The model was formulated under the assumption of a linear magnetic circuit, a symmetrical cylindrical stator and a permanent magnet-type rotor (Fig. 1(a)). The general structure of the

This paper has been accepted for publication in the AEE journal. This is the version which has not been fully edited and content may change prior to final publication.
Citation information: DOI 10.24425/aee.2025.153901

model, for the phase EMF voltage vector $\boldsymbol{e}^{\mathrm{PM}} = \boldsymbol{e}^{\mathrm{PM}}(\theta)$, phase current vector $\boldsymbol{i}$ and the phase generator output voltage vector $\boldsymbol{u}$, can be described in the form:

$$\boldsymbol{e}^{\mathrm{PM}} = \boldsymbol{R}\,\boldsymbol{i} + \boldsymbol{L}(\theta)\frac{\mathrm{d}}{\mathrm{d}t}\boldsymbol{i} + \omega\frac{\partial \boldsymbol{L}(\theta)}{\partial\theta}\,\boldsymbol{i} + \boldsymbol{u}, \tag{1}$$

$$T_m = J\,\frac{\mathrm{d}\omega_m}{\mathrm{d}t} + D\omega_m + T_{\mathrm{cog}}^{\mathrm{PM}} + T_e. \tag{2}$$

The phase EMFs voltage vector $\boldsymbol{e}^{\mathrm{PM}}$ for permanent magnet flux vector $\boldsymbol{\psi}^{\mathrm{PM}}(\theta) = \boldsymbol{\psi}^{\mathrm{PM}}$ and total electromagnetic torque in the generating mode $T_e = T_e(\theta, \boldsymbol{i})$ are given by:

$$\boldsymbol{e}^{\mathrm{PM}} = \omega\,\frac{\partial \boldsymbol{\psi}^{\mathrm{PM}}(\theta)}{\partial\theta}, \quad T_e = \frac{1}{\omega_m}(\boldsymbol{e}^{\mathrm{PM}})^T\boldsymbol{i} + \frac{1}{2}\,\boldsymbol{i}^T\frac{\partial \boldsymbol{L}(\theta)}{\partial\theta}\,\boldsymbol{i}. \tag{3}$$

In Eqs. (1)–(3) vectors and matrices are defined as follows:

$$\boldsymbol{e}^{\mathrm{PM}} = \begin{bmatrix}\boldsymbol{e}^{\mathrm{A}}\\ \boldsymbol{e}^{\mathrm{B}}\\ \boldsymbol{e}^{\mathrm{C}}\\ \boldsymbol{e}^{\mathrm{D}}\end{bmatrix}, \quad \boldsymbol{\Psi}^{\mathrm{PM}} = \begin{bmatrix}\boldsymbol{\Psi}^{\mathbf{A}}\\ \boldsymbol{\Psi}^{\mathbf{B}}\\ \boldsymbol{\Psi}^{\mathbf{C}}\\ \boldsymbol{\Psi}^{\mathbf{D}}\end{bmatrix}, \quad \boldsymbol{i}^{\mathrm{PM}} = \begin{bmatrix}\boldsymbol{i}^{\mathbf{A}}\\ \boldsymbol{i}^{\mathbf{B}}\\ \boldsymbol{i}^{\mathbf{C}}\\ \boldsymbol{i}^{\mathbf{D}}\end{bmatrix}, \quad \boldsymbol{R} = \begin{bmatrix}\boldsymbol{R}^{\mathrm{A}} & \mathbf{0} & \mathbf{0} & \mathbf{0}\\ \mathbf{0} & \boldsymbol{R}^{\mathrm{B}} & \mathbf{0} & \mathbf{0}\\ \mathbf{0} & \mathbf{0} & \boldsymbol{R}^{\mathrm{C}} & \mathbf{0}\\ \mathbf{0} & \mathbf{0} & \mathbf{0} & \boldsymbol{R}^{\mathrm{D}}\end{bmatrix}, \quad \boldsymbol{u} = \begin{bmatrix}\boldsymbol{u}^{\mathbf{A}}\\ \boldsymbol{u}^{\mathbf{B}}\\ \boldsymbol{u}^{\mathbf{C}}\\ \boldsymbol{u}^{\mathbf{D}}\end{bmatrix},$$

$$\boldsymbol{L}(\theta) = \begin{bmatrix}\boldsymbol{L}^{\mathrm{AA}}(\theta) & \boldsymbol{L}^{\mathrm{AB}}(\theta) & \boldsymbol{L}^{\mathrm{AC}}(\theta) & \boldsymbol{L}^{\mathrm{AD}}(\theta)\\ \boldsymbol{L}^{\mathrm{BA}}(\theta) & \boldsymbol{L}^{\mathrm{BB}}(\theta) & \boldsymbol{L}^{\mathrm{BC}}(\theta) & \boldsymbol{L}^{\mathrm{BD}}(\theta)\\ \boldsymbol{L}^{\mathrm{CA}}(\theta) & \boldsymbol{L}^{\mathrm{CB}}(\theta) & \boldsymbol{L}^{\mathrm{CC}}(\theta) & \boldsymbol{L}^{\mathrm{CD}}(\theta)\\ \boldsymbol{L}^{\mathrm{DA}}(\theta) & \boldsymbol{L}^{\mathrm{DB}}(\theta) & \boldsymbol{L}^{\mathrm{DC}}(\theta) & \boldsymbol{L}^{\mathrm{DD}}(\theta)\end{bmatrix}. \tag{4}$$

The following symbols are used in Eqs. (1)–(4): θ is the angle of electrical rotor position, T_m, is the mechanical torque at the generator shaft, ω_m is the mechanical rotor speed, J is the total inertia rotor moment, D is the viscous friction coefficient, $T_{\mathrm{cog}}^{\mathrm{PM}} = T_{\mathrm{cog}}^{\mathrm{PM}}(\theta)$ is the cogging torque. The cogging torque of PM machines produced by magnets can be expanded to a Fourier series. In Eqs. (1)–(3) for channels $k, l \in$ (A, B, C, D), vectors representing phase EMFs voltages $\boldsymbol{e}^k$, phase permanent magnet fluxes $\boldsymbol{\psi}^k$, phase currents $\boldsymbol{i}^k$ and phase output voltages $\boldsymbol{u}^k$ used as sources of energy consumption, as well as matrices of stator resistances $\boldsymbol{R}^k$ and coefficients of self- and mutual inductances $\boldsymbol{L}^{kl}(\theta)$ are defined as follows:

$$\boldsymbol{e}^k = [e_1^k, e_2^k, e_3^k]^T, \quad \boldsymbol{\psi}^k = [\psi_1^{k\,\mathrm{PM}}(\theta), \quad \psi_2^{k\,\mathrm{PM}}(\theta), \quad \psi_3^{k\,\mathrm{PM}}(\theta)]^T, \quad \boldsymbol{i}^k = [i_1^k, i_2^k, i_3^k]^T,$$

$$\boldsymbol{u}^k = [u_1^k, u_2^k, u_3^k]^T, \quad \boldsymbol{R}^k = \mathrm{diag}(R_1^k, R_2^k, R_3^k),$$

$$\boldsymbol{L}^{kl}(\theta) = \begin{bmatrix}L_{11}^{kl}(\theta) & L_{12}^{kl}(\theta) & L_{13}^{kl}(\theta)\\ L_{21}^{kl}(\theta) & L_{22}^{kl}(\theta) & L_{23}^{kl}(\theta)\\ L_{31}^{kl}(\theta) & L_{32}^{kl}(\theta) & L_{33}^{kl}(\theta)\end{bmatrix}. \tag{5}$$

In (5) for $k, l \in$ (A, B, C, D) and $i \in (1, 2, 3)$, $\psi_i^{k\,\mathrm{PM}}(\theta)$ are the permanent magnet fluxes linking the stator windings, $L_{ij}^{kl}(\theta)$ represents the coefficients of self- and mutual inductances. The coefficients $L_{ij}^{kl}(\theta)$ depend on the rotor construction and the internal structure of the generator windings, and can be expanded into a Fourier series. The phase EMFs voltage vectors $\boldsymbol{e}^k$ in Eq.(1) $\boldsymbol{e}^{\mathrm{PM}}$ for channels $k \in$ (A, B, C, D) are defined as follows:

This paper has been accepted for publication in the AEE journal. This is the version which has not been fully edited and content may change prior to final publication.
Citation information: DOI 10.24425/aee.2025.153901

$$\boldsymbol{e}^k = \omega \left[\frac{\partial \psi_1^{k\mathrm{PM}}(\theta)}{\partial \theta}, \frac{\partial \psi_2^{k\mathrm{PM}}(\theta)}{\partial \theta}, \frac{\partial \psi_3^{k\mathrm{PM}}(\theta)}{\partial \theta}\right]^T, \tag{6}$$

where $\omega = \mathrm{d}\theta/\mathrm{d}t = p\omega_m$ is the electrical speed and p is the number of rotor pole pairs. The permanent magnet flux linking each stator winding of the MCBLPMGs follows the trapezoidal profile EMF. The real phase EMF functions can be expressed as Fourier series. The output voltages contained in the vectors $\boldsymbol{u}^k$, $k \in (\mathrm{A}, \mathrm{B}, \mathrm{C}, \mathrm{D})$, supply one or many energy receivers of various types, alternating current (AC) or direct current (DC). For example, these voltages may be associated with a regulated DC load operating in voltage mode. Eqs. (1)–(3) generally constitute a mathematical model of the MCBLPMG in QCO mode or double DCO mode, for example DCO AB + CD or AC + BD mode.

Voltage Eq. (1), phase EMF voltage vector $\boldsymbol{e}^{\mathrm{A}}$ and the electromagnetic torque T_e (3) MCBLPM generator for SCO A mode, i.e. where only channel A is loaded, can be written in the form:

$$\boldsymbol{e}^{\mathrm{A}} = \boldsymbol{R}^{\mathrm{A}}\boldsymbol{i}^{\mathrm{A}} + \boldsymbol{L}^{\mathrm{AA}}(\theta)\frac{\mathrm{d}}{\mathrm{d}t}\boldsymbol{i}^{\mathrm{A}} + \omega\frac{\partial \boldsymbol{L}^{\mathrm{AA}}(\theta)}{\partial \theta}\boldsymbol{i}^{\mathrm{A}} + \boldsymbol{u}^{\mathrm{A}}, \tag{7}$$

$$\boldsymbol{e}^{\mathrm{A}} = \omega\frac{\partial \boldsymbol{\psi}^{\mathrm{A}}(\theta)}{\partial \theta}, \quad T_e = \frac{1}{\omega_m}(\boldsymbol{e}^{\mathrm{A}})^T\boldsymbol{i}^{\mathrm{A}} + \frac{1}{2}(\boldsymbol{i}^{\mathrm{A}})^T\frac{\partial \boldsymbol{L}^{\mathrm{AA}}(\theta)}{\partial \theta}\boldsymbol{i}^{\mathrm{A}}, \tag{8}$$

where vectors and matrices are defined in (5) and (6). Additional constraints on voltages and currents are imposed by the arrangement of generator phase windings in a star configuration (Y). The relationship of line (L) and phase voltages and currents in SCO A mode, can be written as:

$$\boldsymbol{e}_{\mathrm{L}}^{\mathrm{A}} = \left[e_{12}^{\mathrm{A}}, e_{23}^{\mathrm{A}}, e_{31}^{\mathrm{A}}\right]^T = \boldsymbol{K}_{\mathrm{Y}}\boldsymbol{e}^{\mathrm{A}}, \quad \boldsymbol{u}_{\mathrm{L}}^{\mathrm{A}} = \left[u_{12}^{\mathrm{A}}, u_{23}^{\mathrm{A}}, u_{31}^{\mathrm{A}}\right]^T = \boldsymbol{K}_{\mathrm{Y}}\boldsymbol{u}^{\mathrm{A}},$$
$$\boldsymbol{i}_{\mathrm{L}}^{\mathrm{A}} = \boldsymbol{i}^{A} = \left[i_1^{\mathrm{A}}, i_2^{\mathrm{A}}, i_3^{\mathrm{A}}\right]^T, \quad \boldsymbol{K}_{\mathrm{Y}} = \begin{bmatrix} 1 & -1 & 0 \\ 0 & 1 & -1 \\ -1 & 0 & 1 \end{bmatrix}. \tag{9}$$

Connecting the phase windings of a given channel A into a star (Y) without a neutral wire imposes constraint equations for currents of the form:

$$\begin{bmatrix} 1 & 1 & 1 \end{bmatrix}\ \boldsymbol{i}_{\mathrm{L}}^{\mathrm{A}} = 0. \tag{10}$$

Eqs. (7)–(10) constitute the mathematical model of the MCBLPM generator in SCO A mode for the star (Y) connection.

4. Numerical calculations and laboratory test

A numerical model was constructed for finite element method (FEM) calculations using the commercial Ansys Electronics software program. The calculations in Subchapter 4.1 were performed with a rotational speed approaching zero ($n \approx 0$ rpm). The remaining tests were carried out with a rotational speed of $n = 1500$ rpm. To accommodate an AC/DC system with a DC voltage source ($U_{\mathrm{dc}} = \mathrm{const}$), a circuit model was used. This circuit model was strongly coupled with the MCBLPMG field model. The scope of the calculations was limited to SCO for

This paper has been accepted for publication in the AEE journal. This is the version which has not been fully edited and content may change prior to final publication.
Citation information: DOI 10.24425/aee.2025.153901

each of the variants discussed in Subchapter 2.2. Laboratory tests were carried out under comparable conditions.

4.1. Self- and mutual inductances

To complete the coefficients of the inductance matrix $\boldsymbol{L}^{kl}(\theta)$ as defined in Eq. (5), the self- and mutual inductances within the SCO were determined. The calculations were carried out over one electrical period. The results of the calculations for Var I are presented in Fig. 4.

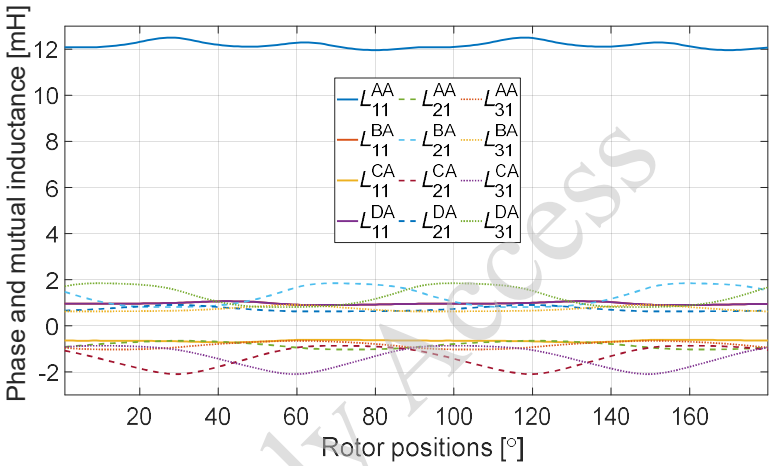

Fig. 4. Self- and mutual inductances vs rotor positions – numerical test of Var I

The remaining two variants prove identical mutual magnetic couplings values and were therefore excluded from the paper. The self-inductance remains nearly constant because of the surface-mounted permanent magnets, which allows for the exclusion of issues related to the generation of the reluctance component of the electromagnetic torque. In each variant, there are four dominant magnetic couplings, consisting of two positive and two negative components. Table 2 presents a summary of the obtained results concerning the dominant mutual inductances.

Table 2. Dominant mutual inductances for SCO

Mutual inductance/Var	Var I	Var II	Var III
$L^{BA}{}_{11}$	~0	~0	~0
$L^{CA}{}_{11}$	~0	~0	~0
$L^{DA}{}_{11}$	~0	~0	~0
$L^{AA}{}_{21}$	~0	-	+
$L^{BA}{}_{21}$	+	~0	-

This paper has been accepted for publication in the AEE journal. This is the version which has not been fully edited and content may change prior to final publication.
Citation information: DOI 10.24425/aee.2025.153901

$L^{CA}{}_{21}$	-	~0	~0
$L_{DA}{}^{21}$	~0	+	~0
$L^{AA}{}_{31}$	~0	~0	+
$L^{BA}{}_{31}$	~0	~0	~0
$L^{CA}{}_{31}$	-	-	~0
$L^{DA}{}_{31}$	+	+	-

The remaining mutual magnetic couplings are of secondary importance and can be determined from the rotor position angle. Furthermore, only Var III ensures the most notable magnetic separation between channels A and C, which represents a significant advantage of this variant. In Var I, the magnetic couplings are dominant in relation to all channels. The magnetic couplings between Var II and channel B are relatively minor.

4.2. Induced voltages

To analyse the three configurations, the induced voltages were determined. For the Var I configuration, the induced phase and line-to-line voltages are illustrated in Figs. 5, and 6. The results of the numerical tests were compared with the laboratory tests detailed in reference [40]. The experiment was conducted at a rotational speed of 1500 rpm.

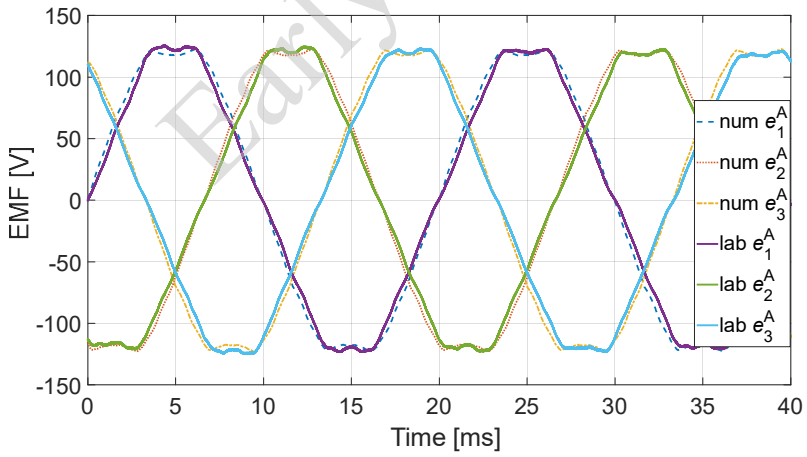

Fig. 5. EMF – numerical and laboratory test of Var I

This paper has been accepted for publication in the AEE journal. This is the version which has not been fully edited and content may change prior to final publication.
Citation information: DOI 10.24425/aee.2025.153901

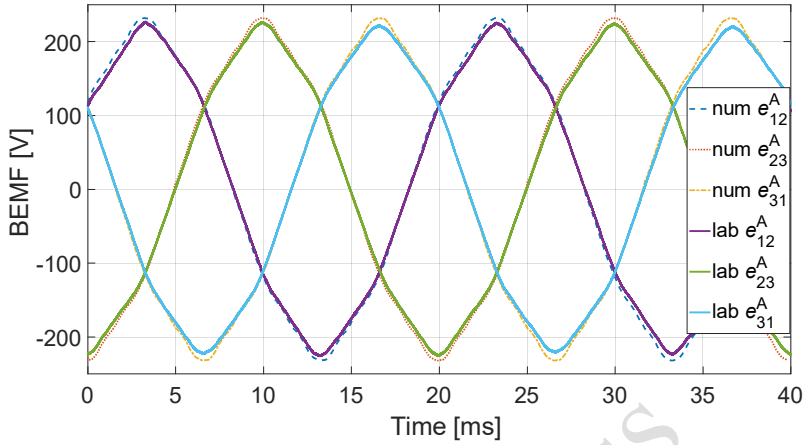

Fig. 6. Line-to-line EMF – numerical and laboratory test of Var I

Variants II and III displayed identical induced voltages waveforms. This indicates that the selection of channel configurations has no impact on the induced voltage waveforms. The results of the laboratory tests are comparable to those obtained from the numerical tests. However, discrepancies in the induced voltage waveforms become evident under laboratory conditions. These differences are due to imperfections in the manufacturing process, particularly regarding the mounting of the permanent magnets (e.g., the use of a pseudoskew).

4.3. Current and voltage waveforms

The numerical tests were conducted at a single operating point, with identical generator load conditions for each variant's configuration. Only the SCO mode was tested. The numerical test was carried out at a speed of 1500 rpm, assuming that the AC/DC system would be connected to a constant voltage source (U_{dc} = const). For the experiment, it was assumed that the battery voltage would be 150 V. For Var I this corresponds to an output power of 750 W. In SCO mode, the machine should be able to operate at this power for several minutes. The phase current waveforms for the tested channel A are shown in Fig. 7, and the receiver current (i_{DC}) is shown in Fig. 8.

This paper has been accepted for publication in the AEE journal. This is the version which has not been fully edited and content may change prior to final publication.
Citation information: DOI 10.24425/aee.2025.153901

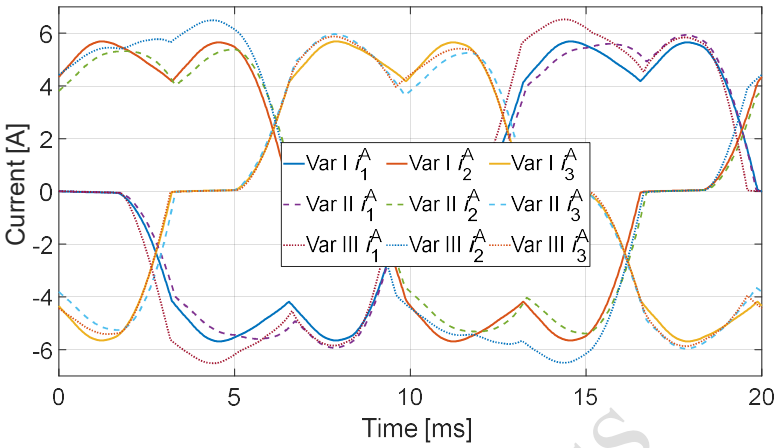

Fig. 7. Phase current waveforms – Var I, II and III

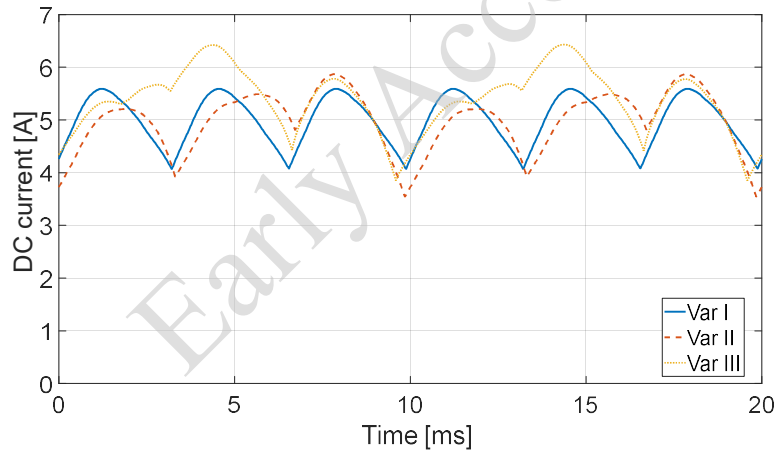

Fig. 8. DC current waveforms – Var I, II and III

Table 3 presents a summary of the results obtained for the phase currents and the receiver current for all analysed variants.

Table 3. Numerical tests results for phase currents and receiver current

Value/Var	Var I	Var II	Var III
RMS of phase current i_1^A [A]	4.04	4.15	4.52
RMS of phase current i_1^A [A]	4.04	3.89	4.51
RMS of phase current i_1^A [A]	4.04	4.03	4.04

This paper has been accepted for publication in the AEE journal. This is the version which has not been fully edited and content may change prior to final publication.
Citation information: DOI 10.24425/aee.2025.153901

DC current $i_{DC\_av}^{A}$ [A]	5.00	4.97	5.38

The variant selected affects the generator current waveforms in SCO operation. The greatest impact is observed in the case of Var III, which also influences the current waveforms in the DC circuit. Var I ensures complete symmetry of the phase currents, while Var III introduces the greatest asymmetry by grouping all channel phases at a half-pitch of the slot. However, the asymmetry introduced by mutual magnetic couplings remains at an acceptable level. The voltage waveforms (phase and line-to-line) at the generator output are shown in Figs. 9 and 10.

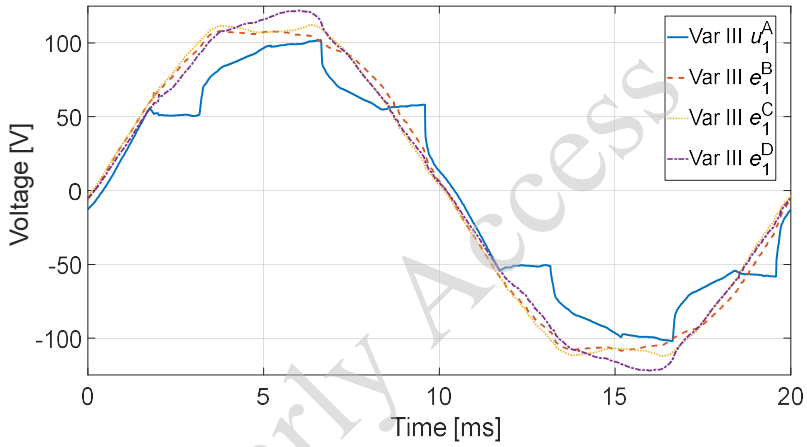

Fig. 9. Phase voltage and EMF waveforms – Var III

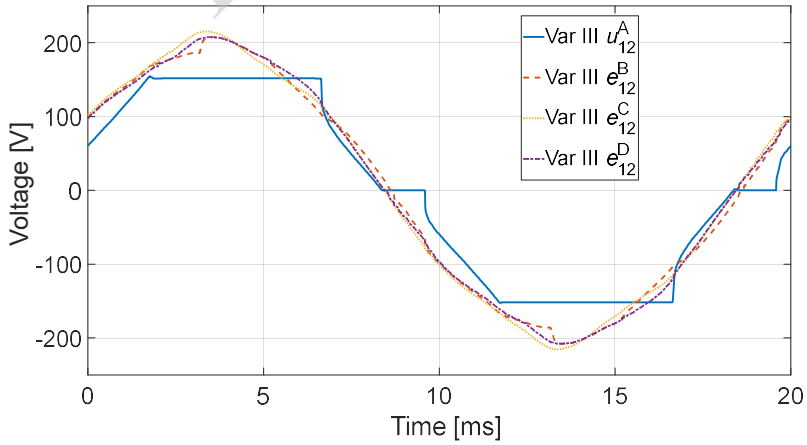

Fig. 10. Line-to-line voltage and EMF waveforms –Var III

This paper has been accepted for publication in the AEE journal. This is the version which has not been fully edited and content may change prior to final publication.
Citation information: DOI 10.24425/aee.2025.153901

An overview of the phase voltage RMS values is provided in Table 4, while the corresponding line-to-line voltage values are presented in Table 5. The results of the calculations for channel A are highlighted in bold in Tables 4 and 5.

Table 4. Numerical test results for phase voltages

Value/Var	Var I	Var II	Var III
RMS of phase voltage U_1^A [V]	**68.51**	**68.71**	**68.35**
RMS of phase EMF E_1^B [V]	84.66	83.91	81.77
RMS of phase EMF E_1^C [V]	83.09	81.91	82.94
RMS of phase EMF E_1^D [V]	82.37	82.79	83.90
RMS of phase voltage U_2^A [V]	**68.35**	**68.64**	**69.26**
RMS of phase EMF E_2^B [V]	84.41	81.98	80.58
RMS of phase EMF E_2^C [V]	82.86	82.53	83.03
RMS of phase EMF E_2^D [V]	82.12	84.46	82.19
RMS of phase voltage U_3^A [V]	**68.34**	**67.80**	**65.70**
RMS of phase EMF E_3^B [V]	84.28	82.65	82.92
RMS of phase EMF E_3^C [V]	82.84	83.71	82.17
RMS of phase EMF E_3^D [V]	82.08	83.86	86.14

Table 5. Numerical test results for line-to-line voltages

Value\Var	Var I	Var II	Var III
RMS of phase voltage U_{12}^A [V]	**118.5**	**119.2**	**118.8**
RMS of phase EMF E_{12}^B [V]	146.3	143.3	140.5
RMS of phase EMF E_{12}^C [V]	143.7	141.6	143.9
RMS of phase EMF E_{12}^D [V]	142.5	145.1	142.6
RMS of phase voltage U_{23}^A [V]	**118.2**	**117.8**	**116.8**
RMS of phase EMF E_{23}^B [V]	145.8	142.6	140.8
RMS of phase EMF E_{23}^C [V]	143.3	144.9	142.7
RMS of phase EMF E_{23}^D [V]	142.1	145.3	147.1
RMS of phase voltage U_{31}^A [V]	**118.5**	**118.1**	**116.3**
RMS of phase EMF E_{31}^B [V]	146.2	144.4	143.2
RMS of phase EMF E_{31}^C [V]	143.7	143.0	142.9

This paper has been accepted for publication in the AEE journal. This is the version which has not been fully edited and content may change prior to final publication.
Citation information: DOI 10.24425/aee.2025.153901

RMS of phase EMF $E_{31}{}^{D}$ [V]	142.5	144.1	147.1

The influence of the operating channel A on the induced voltages in the remaining channels (B, C, and D) is noticeable, but its practical significance is marginal. Similar results were obtained for the two phases. This conclusion holds for Variants I and II. This is important for diagnostic methods based on voltage signals in multichannel operations as it enables the operating status of each channel to be analysed independently.

4.4. Efficiency and external characteristics

Based on the numerical calculations (for all variants) and laboratory tests, the relationship between efficiency and output power was determined. This relationship was then used to calculate the efficiency under numerical conditions:

$$\eta = \frac{P_{\text{out}}}{P_{\text{out}}+\Delta P_{\text{Cu}}+\Delta P_{\text{Fe}}+\Delta P_{\text{mag}}+\Delta P_{\text{mech}}} \cdot 100, \tag{11}$$

where: $P_{\text{out}} = U_{\text{dc}} * I_{\text{dcav}}$ is the output power, P_{Cu} stands for the copper losses, ΔP_{Fe} represents the core losses, ΔP_{mag} represents the permanent magnet losses, ΔP_{mech} means the total mechanical losses. In numerical calculations, core losses, permanent magnet losses and mechanical losses must be accounted for determining efficiency (Eq. 11). For laboratory tests, Eq. 11 is simplified to the following form:

$$\eta = \frac{P_{\text{out}}}{P_{\text{in}}} \cdot 100, \tag{12}$$

where P_{in} is the input power.

Laboratory tests were performed only for Var I and Var III. A comprehensive overview of the findings is presented in Fig. 11. For optimal generator performance, it is essential to consider the external characteristics. To evaluate the impact of Var I, II and III on these characteristics, the dependence of the phase voltage on the phase current for each phase was determined. The results are shown in Figs. 12–14.

This paper has been accepted for publication in the AEE journal. This is the version which has not been fully edited and content may change prior to final publication.
Citation information: DOI 10.24425/aee.2025.153901

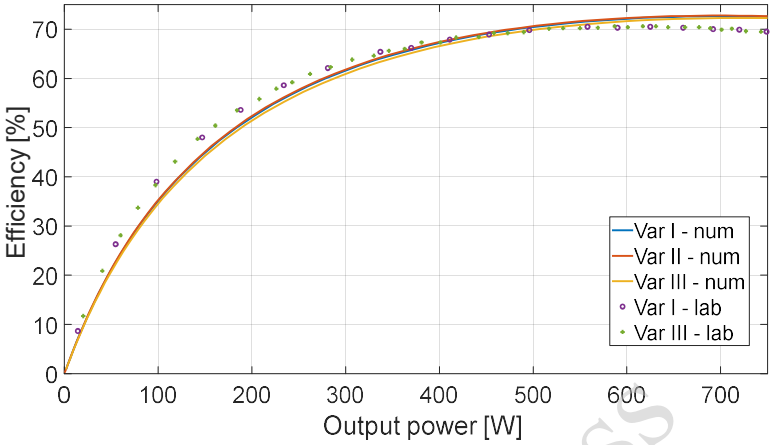

Fig. 11. Efficiency vs output power – Var I, II and III, numerical and laboratory tests

In general, the achieved generator efficiency was found to be in good agreement with the expected value. The specific variant does not affect the efficiency of the generator's energy processing in SCO mode, as confirmed by both numerical studies and laboratory tests. According to the required power of 750 W under SCO conditions, it was observed that maximum efficiency is reached at a power level of approximately 620 W (laboratory test). In the numerical calculations, maximum efficiency is observed at the required output power. However, it should be noted that the numerical calculations do not account for the increase in winding resistance. The winding temperature rises to approximately twice its original value as a result of operation in the overload range. It is important to emphasise that a generator operating in the SCO mode is considered to be in a critical operating state, which allows the generator to operate within a defined period, such as, for instance until the generator is destroyed. Nevertheless, the examined generator is capable of maintaining the required power output during continuous operation.

This paper has been accepted for publication in the AEE journal. This is the version which has not been fully edited and content may change prior to final publication.
Citation information: DOI 10.24425/aee.2025.153901

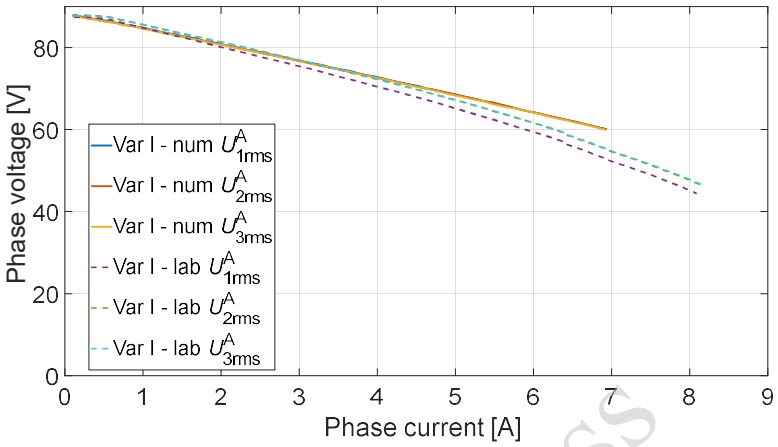

Fig. 12. Phase voltage vs phase current – Var I, numerical and laboratory test

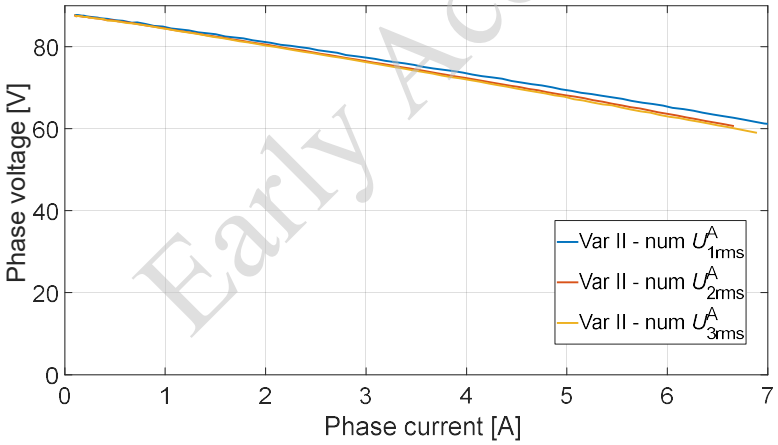

Fig. 13. Phase voltage vs phase current – Var II, numerical test

This paper has been accepted for publication in the AEE journal. This is the version which has not been fully edited and content may change prior to final publication.
Citation information: DOI 10.24425/aee.2025.153901

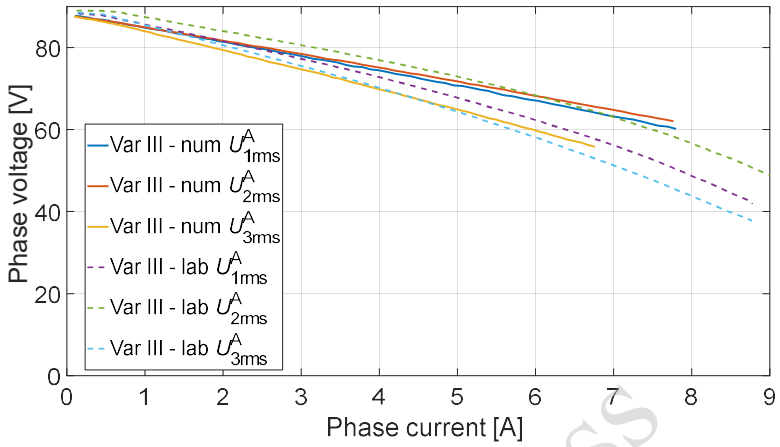

Fig. 14. Phase voltage vs phase current –Var III, laboratory test

Furthermore, the vibration velocity of one of the bearing shield housings was documented during the experimental procedure. In such cases, the effective value of the vibration velocity (Fig. 15) is not the only parameter of interest; the maximum value is also important to consider (Fig. 16).

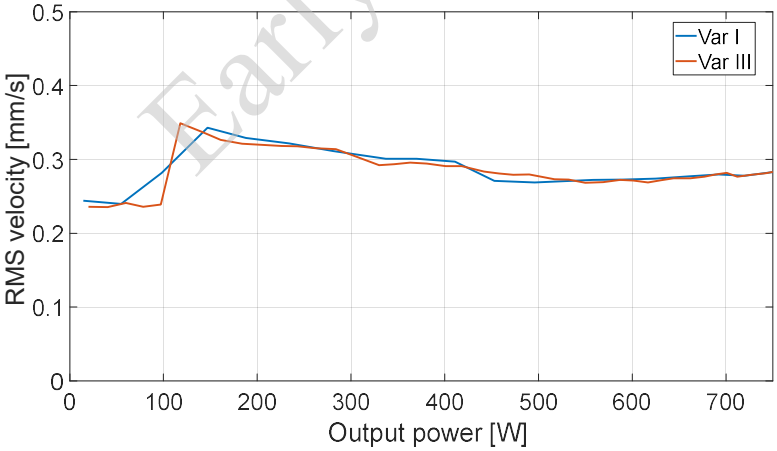

Fig. 15. RMS of velocity vs output power –Var I and III, laboratory test

This paper has been accepted for publication in the AEE journal. This is the version which has not been fully edited and content may change prior to final publication.
Citation information: DOI 10.24425/aee.2025.153901

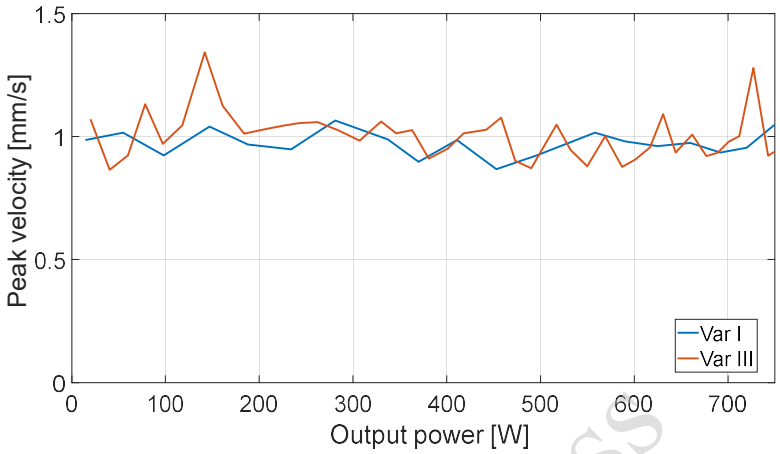

Fig. 16. Peak velocity vs output power –Var I and III, laboratory test

In Var I, the operation is symmetrical, achieving a state of perfect numerical symmetry. However, in the laboratory tests, a slight asymmetry was observed (Fig. 12). This outcome can be attributed to performance factors. The results of both the numerical and laboratory tests show that Var III introduces the highest degree of internal asymmetry. In the case of Var III, it is evident that the individual phases experience unequal loaded, as shown in both Fig. 14 and Fig. 7. Under laboratory conditions, a reduction in the rigidity of the external characteristics was observed. This is due to an increase of the windings' resistance during the tests, caused by winding heating.

Regarding the effective value of the vibration velocity, no significant differences were observed between Variants I and III (Fig. 15). However, when considering the maximum vibration velocity values (Fig. 16), a noticeable discrepancy is evident. Compared to the other variants, Var III displays higher maximum of vibration velocity values when the generator operates in SCO mode. However, these results confirm that Var III is more susceptible to vibrations.

5. Summary

This paper presents an analysis of novel winding configuration solutions designed for BLPMG multichannel operations. The use of an exceptionally very short-pitch distributed winding in the BLPMG enables the realisation of Var III, which offers improved electrical separation between the channels of individual phases. In the event of a winding fault (e.g. a partial short circuit), this configuration helps to minimise potential damage to adjacent channels. Compared to the Var I configuration, which provides complete symmetry, the Var III configuration exhibits a greater degree of asymmetry due to magnetic couplings. In each of the

This paper has been accepted for publication in the AEE journal. This is the version which has not been fully edited and content may change prior to final publication.
Citation information: DOI 10.24425/aee.2025.153901

SCO variants analysed, the prototype generator demonstrated the ability to operate at the required power level. Moreover, the Var III configuration allows for the generation of the required output power with essentially the same efficiency. However, a slight deterioration in vibroacoustic conditions is observed with Var III. Further research will focus on the multichannel operation of the BLPMG, with particular emphasis on the Var III configuration.

References

[1] Boldea I., *Electric generators and motors: An overview*, CES Transactions on Electrical Machines and Systems, vol. 4, no. 1, pp. 3–14 (2017), DOI: 10.23919/TEMS.2017.7911104.
[2] He C., Wu T., *Analysis and design of surface permanent magnet synchronous motor and generator*, CES Transactions on Electrical Machines and Systems, vol. 3, no. 1, pp. 94–100 (2019), DOI: 10.30941/CESTEMS.2019.00013.
[3] Gramaticov P., *Electric motor-generators for unmanned aerial vehicles*, Aerospace Research in Bulgaria, vol. 29 (2017), DOI: 10.3897/arb.v30.e10.
[4] Wang B., Vakil G., Liu Y., Yang T., Zhang Z., Gerada C., *Optimization and Analysis of a High Power Density and Fault Tolerant Starter–Generator for Aircraft Application*, Energies, vol. 14, no. 1 (2021), DOI: 10.3390/en14010113.
[5] Zhang Z., Huang J., Jiang Y., Geng W., Xu Y., *Overview and analysis of PM starter/generator for aircraft electrical power systems*, CES Transactions on Electrical Machines and Systems, vol. 1, no. 2, pp. 117–131 (2017), DOI: 10.23919/TEMS.2017.7961293.
[6] Wang B., Vakil G., Liu Y., Yang T., Zhang Z., Gerada C., *Optimization and Analysis of a High Power Density and Fault Tolerant Starter–Generator for Aircraft Application*, Energies, vol. 14, no. 1 (2021), DOI: 10.3390/en14010113.
[7] Kumar R.R., Kumari A., Dutta S., Kumar K., *Design and Characteristic Evaluation of a Novel Dual Rotor Multi-layer Magnetic Pole Five-Phase Permanent Magnet Synchronous Generator for Marine Power Application*, IEEE International Conference on Power Electronics, Drives and Energy Systems (PEDES) (2020), DOI: 10.1109/PEDES49360.2020.9379624.
[8] Jiang X., Zhang L., Li F., Zhao Z., *Design and Analysis of a Highly Reliable Permanent Magnet Synchronous Machine for Flywheel Energy Storage*, Machines, vol. 12, no. 9 (2024), DOI: 10.3390/machines12090655.
[9] Chung D.-W., You Y.-M., *Cogging Torque Reduction in Permanent-Magnet Brushless Generators for Small Wind Turbines*, Journal of Magnetics, vol. 20, pp. 176–185 (2015), DOI: 10.4283/JMAG.2015.20.2.176.
[10] Gwóźdź M. Krystykowiak M., Ciepliński Ł., Strzelecki R., *A Wind Energy Conversion System Based on a Generator with Modulated Magnetic Flux*, Energies, vol. 13, no. 12 (2020), DOI: 10.3390/en13123285.
[11] Ullah W., Khan F., Hussain S., *A Novel Dual Rotor Permanent Magnet Flux Switching Generator for Counter Rotating Wind Turbine Applications*, IEEE Access, vol. 10, pp. 16456–16467 (2022), DOI: 10.1109/ACCESS.2022.3149895.
[12] Hao L., Yakai S., Chunlan B., Guofeng H., Xiaoju Y., *A dual-stator brushless doubly-fed generator for wind power application*, Archives of Electrical Engineering, vol. 72, no. 4, pp. 1073–1087 (2023), DOI: 10.24425/aee.2023.147427.
[13] Levi E., *Multiphase electric machines for variable-speed applications*, IEEE Trans. Ind. Electron., vol. 55, no. 5, pp. 1893–1909 (2008), DOI: 10.1109/TIE.2008.918488.
[14] Levi E., Barrero F., Duran M.J., *Multiphase machines and drives – Revisited*, IEEE Transactions on Industrial Electronics, vol. 63, iss. 1, pp. 429–432 (2016), DOI: 10.1109/TIE.2015.2493510.

This paper has been accepted for publication in the AEE journal. This is the version which has not been fully edited and content may change prior to final publication.
Citation information: DOI 10.24425/aee.2025.153901

[15] Yepes A.G., Lopez O., Gonzales-Prieto I., Duran M.J., Doval-Gandoy J., *A Comprehensive Survey on Fault Tolerance in Multiphase AC Drives, Part 1: General Overview Considering Multiple Fault Types*, Machines, vol. 10, no. 3 (2022), DOI: 10.3390/machines10030208.

[16] Parsa L., Toliyat H.A., *Multi-phase permanent magnet motor drives*, 38th IAS Annual Meeting on Conference Record of the Industry Applications Conference (2003), DOI: 10.1109/IAS.2003.1257532.

[17] Gonzalez-Prieto I., Duran M.J., Garcia-Entrambasaguas P., Bermudez M., *Field-Oriented Control of Multiphase Drives with Passive Fault Tolerance*, IEEE Transactions on Industrial Electronics, vol. 67, iss. 9, pp. 7228–7238 (2020), DOI: 10.1109/TIE.2019.2944056.

[18] Iftikar M.H., Byoung-Gun P., Ji-Won K., *Design and Analysis of a Five-Phase Permanent-Magnet Synchronous Motor for Fault-Tolerant Drive*, Energies, vol. 14, no. 2 (2021), DOI: 10.3390/en14020514.

[19] Huang C., Zhou L., Cao Z., Yao G., *Fault-Tolerant Control Strategy with Asymmetric Phase Currents for Single to Four-Phase Open-Circuit Faults of Six-Phase PMSM*, Energies, vol. 14, no. 11 (2021), DOI: 10.3390/en14113163.

[20] Fireţeanu V., Dumitru C., *Finite Element Analysis of Multiphase Permanent Magnet Synchronous Motors with the Same Stators of Analogue 3-phase, 5-phase, 7-phase and 9-phase Induction Motors*, International Conference on Applied and Theoretical Electricity (ICATE) (2021), DOI: 10.1109/ICATE49685.2021.9465021.

[21] Darijevic M., Jones M., Dordevic O., Levi E., *Decoupled PWM Control of a Dual-Inverter Four-Level Five-Phase Drive*, IEEE Transactions on Power Electronics, vol. 32, iss. 5, pp. 3719–3730 (2017), DOI: 10.1109/TPEL.2016.2582703.

[22] Nekoubin A., Soltani J., Dowlatshan M., *Multi-objective design optimization of five-phase fractional-slot concentrated-winding surface-mounted permanent-magnet machine*, Archives of Electrical Engineering, vol. 69, no. 4, pp. 873–889 (2020), DOI: 10.24425/aee.2020.134636.

[23] Akay A., Lefley P., Kansara M., *Open-Circuit Fault-Tolerant Control for a Five-Phase Permanent Magnet Synchronous Machine Drive*, 7th International Conference on Electrical and Electronics Engineering (ICEEE) (2020), DOI: 10.1109/ICEEE49618.2020.9102486.

[24] Zhao J., Lu Z., Han Q., Wang L., *Design and Analysis of a Novel Six-Phase Axial Switched-Flux Permanent Magnet Machine with Different Winding Configuration*, IEEE Transactions on Magnetics, vol. 59 (2023), DOI: 10.1109/TMAG.2023.3287558.

[25] Zhao J., Xie W., *Fault-Tolerant Control Strategy of Five-Phase Permanent Magnet Synchronous Generator*, 6th International Conference on Electrical Engineering and Green Energy (CEEGE) (2023), DOI: 10.1109/CEEGE58447.2023.10246742.

[26] Chukwuemeka C.A., *Performance comparison of double stator permanent magnet machines*, Archives of Electrical Engineering, vol. 71, no. 4, pp. 829–850 (2022), DOI: 10.24425/aee.2022.142111.

[27] Rubino S., Dordevic O., Bojoi R., Levi E., *Modular Vector Control of Multi-Three-Phase Permanent Magnet Synchronous Motors*, IEEE Transactions on Industrial Electronics, vol. 68, iss. 10 (2021), DOI: 10.1109/TIE.2020.3026271.

[28] Shchur I., Jancarczyk D., *Electromagnetic Torque Ripple in Multiple Three-Phase Brushless DC Motors for Electric Vehicles*, Electronics, vol. 10, no. 24 (2021), DOI: 10.3390/electronics10243097.

[29] Wang W., Zhang J., Cheng M., Li S., *Fault-Tolerant Control of Dual Three-Phase Permanent-Magnet Synchronous Machine Drives Under Open-Phase Faults*, IEEE Transactions on Power Electronics, vol. 32, iss. 3, pp. 2052–2063 (2017), DOI: 10.1109/TPEL.2016.2559498.

This paper has been accepted for publication in the AEE journal. This is the version which has not been fully edited and content may change prior to final publication.
Citation information: DOI 10.24425/aee.2025.153901

[30] Chen Q., Xu D., Xu L., Wang J., Lin Z., Zhu X., *Fault-Tolerant Operation of a Novel Dual-Channel Switched Reluctance Motor Using Two 3-Phase Standard Inverters*, IEEE Transactions on Applied Superconductivity, vol. 28, no. 3 (2018), DOI: 10.1109/TASC.2018.2799838.

[31] Ding W., *Comparative Study on Dual-Channel Switched Reluctance Generator Performances Under Single- and Dual-Channel Operation Modes*, IEEE Transactions on Energy Conversion, vol. 27, no. 3, pp. 680–688 (2012), DOI: 10.1109/TEC.2012.2194497.

[32] Wang Z., Liu B., Guan L., Zhang Y., Cheng M., Zhang B., Xu L., *A Dual-Channel Magnetically Integrated EV Chargers Based on Double-Stator-Winding Permanent-Magnet Synchronous Machines*, IEEE Transactions on Industry Applications, vol. 55, no. 2, pp. 1941–1953 (2019), DOI: 10.1109/TIA.2018.2879869.

[33] Korkosz M., Sztajmec E., Prokop J., *Electromagnetic Performance Analysis of a Multichannel Permanent Magnet Synchronous Generator*, Energies, vol. 16, no. 23 (2023), DOI: 10.3390/en16237816.

[34] Młot A., Korkosz M., Lechowicz A., Podhajecki J., Rawicki S., *Electromagnetic analysis, efficiency map and thermal analysis of an 80-kW IPM motor with distributed and concentrated winding for electric vehicle applications*, Archives of Electrical Engineering, vol. 71, no. 4, pp. 981–1002 (2022), DOI: 10.24425/aee.2022.142120.

[35] Roth C., Dakaju G., Gerold J., Greifelt A., Gerling D., *Distributed Windings with Flux Barriers Applied to PM Wind Generators*, 25th International Conference on Electrical Machines and Systems (ICEMS) (2022), DOI: 10.1109/ICEMS56177.2022.9983167.

[36] Qio H., Zhang Y., Yang C., Yi R., *Performance analysis and comparison of PMSM with concentrated winding and distributed winding*, Archives of Electrical Engineering, vol. 69, no. 2, pp. 303–317 (2020), DOI: 10.24425/aee.2020.133027.

[37] Yan Z., Si J., Nie R., Cheng Z., Dong L., Li Z., *Comparative Analysis of Tubular Permanent Magnet Linear Generator with Equidirectional Toroidal Windings and Conventional Toroidal Windings*, IEEE Transactions on Industry Applications, vol. 58, iss. 4, pp. 4614–4624 (2022), DOI: 10.1109/TIA.2022.3172238.

[38] Erd N., Binder A., *Concentrated Windings for Wind Generators with Solid Rotor Iron and Redundant Feeding*, International Conference on Electrical Machines (ICEM) (2020), DOI: 10.1109/ICEM49940.2020.9270688.

[39] Diana M., Lundmark S.T., Thiringer T., *High Voltage Direct Drive Generators with Multiphase Single Layer Fractional Slot Concentrated Windings*, International Conference on Electrical Machines (ICEM) (2020), DOI: 10.1109/ICEM49940.2020.9270963.

[40] Korkosz M., Krzywdzińska-Kornak K., Parfianowicz K., Prokop J., Shchur I., *Design and Analysis of the Characteristics of a Brushless Permanent Magnet Motor for Critical Drive*, International Conference on Electrical Drives and Power Electronics (EDPE) (2023), DOI: 10.1109/EDPE58625.2023.10274060.